# Hierarchically Porous Nickel/Carbon Composite Monoliths Prepared by Sol-Gel Method from an Ionic Precursor

Yasuki KIDO, Kazuki NAKANISHI,* Nao OKUMURA, Kazuyoshi KANAMORI

Department of Chemistry, Graduate School of Science, Kyoto University, Kitashirakawa, Sakyo-ku, Kyoto 606-8502, Japan

Corresponding author: Prof. Kazuki NAKANISHI

Department of Chemistry, Graduate School of Science, Kyoto University, Kitashirakawa, Sakyo-ku, Kyoto 606-8502, Japan.

Tel/Fax: +81 75 753 2925, E-mail: kazuki@kuchem.kyoto-u.ac.jp

**Abstract**

Utilizing a facile sol-gel reaction accompanied by phase separation, rigid monolithic nickel hydroxide-based xerogels and nickel/carbon composites with hierarchical porosity have been successfully fabricated. In the synthetic route starting from nickel chloride as a nickel precursor, trimethylene oxide acts as a gelation initiator to increase pH in a reaction solution. In addition, poly(acrylic acid) plays a double role as a phase separation inducer and as a co-constituent with nickel

hydroxide to comprise continuous gel skeletons in the micrometer range. As a result, obtained xerogels possess well-defined macropores evidenced by microscopy observation and mercury porosimetry. Subsequent heat-treatment in air led to the crystallization of NiO at 300 ºC, while calcination under argon flow brought about the formation of nickel/carbon (Ni/C) composites with hierarchical pores and large specific surface area at temperatures higher than 300 ºC. This is the first report on the preparation of rigid monolithic xerogels and metal/carbon composite with well-defined macropores based on a metal salt precursor containing “divalent” cation.

**Keywords**

Nickel/Carbon composite; Sol-gel; Phase separation; Monolith; Hierarchically porous

## 1. Introduction

Nickel oxides, including those with non-stoichiometry, $NiO_{1+}$ , are technologically important compounds utilized as semiconductors, gas sensors, and catalyst supports owing to their specific chemical properties [1-3]. For the better tuning of their properties, it is essential to control morphology, particle size, crystallinity, and surface area as well as the electronic defects [4,5]. On the other hand, metal/carbon composite materials are widely used as catalysts, electrodes, and hydrogen storage materials [6-10]. Numerous works have been so far performed on nickel hydroxide-based materials aiming at a precise control over morphology, such as particles, nanorods or whiskers, and thin films [11-19]. For example, porous nickel oxide exhibits high electrochemical capacitive performance because it is enhanced by the material's nanostructure such as high specific surface area and fast redox reactions [20]. Only a few researches, however, have been carried out to prepare porous materials in a "monolithic" form. Among various synthetic strategies to obtain porous monolithic materials, a sol-gel approach accompanied by phase separation is one of the well-established routes [21]. Materials obtained by this technique have been utilized for catalysts and separation media (monolithic columns for high-performance liquid chromatography (HPLC)) since they have both well-defined macropores in the micrometer range which act as a pathway for the mobile phase, and meso/micropores to provide large surface areas where the external molecules will efficiently interact [22,23]. The sol-gel reaction generally utilizes metal alkoxide as a precursor which is hydrolyzed and polycondensed to form gel

networks. On the other hand, the synthetic route using metal salts as a precursor has been actively explored especially during this decade, where epoxide plays a central role in inducing homogeneous gelation. Organic cyclic ethers such as propylene oxide act as a gelation initiator to induce a moderate increase in pH of aqueous solution containing hydrated metal cations [24]. The facile and versatile process for obtaining monolithic gels from metal salts has proven to be effective in an extended materials composition including oxides of transition and main group metals [25]. Recently, this unique sol-gel method has been combined with the above-mentioned phase-separation technique to produce co-continuous macroporous monolithic gels composed of tri-, di-, and mono-valent metal cations [26-29]. In the reaction using organic cyclic ethers, it is known that the acidity of metal cation ($M^{X+}$) estimated by its valence ($X$) dominates the gelation behavior. The rate of polycondensation, that of network formation, and precipitation kinetics are all governed by the rate of pH change in the solution, where the reactivity of metal salts toward hydrolysis decreases in the order of $X = 4 > 3 > 2$ [25]. Therefore, it is not easy to obtain monolithic gels based on the smaller valence metal cation than those with tri- or tetra-valence because of the increasing difficulty in promoting homogeneous gelation. There have been effectively no reports on fabricating porous divalent monolithic oxide gels except the case of fragile aerogels [31,32]. Synthesis of the divalent metal oxides requires precise controls over the gelation process; for example, concentrations of solvents, gelation initiator, and additives should be finely tuned to promote network formations rather than dispersed precipitates. Herein, we demonstrate

the preparation of rigid monolithic nickel hydroxide-based xerogels and metal nickel/carbon composites with controlled macroporous morphology from nickel chloride hexahydrate ($NiCl_2$•$6H_2O$) as a nickel source. Here trimethylene oxide, TMO, is used as a gelation initiator to promote moderate gelation parallel to phase separation to form monolithic gels with homogeneous structure. In addition, poly(acrylic acid) acts both as the phase separation inducer and as the network-forming constituent that supports the gel network to produce monolithic rigid gels with co-continuous skeletons [33]. We investigated the effects of starting compositions and heat-treatment conditions on gelation, morphology, and crystalline phases. To the best of our knowledge, the present research is the first report on the synthesis of rigid monolithic xerogels based on "divalent" metal hydroxide with well-defined macropores.

## 2. Experimental Section

### 2.1. Preparation

Nickel chloride hexahydrate ($NiCl_2$•$6H_2O$, Sigma-Aldrich, 99 %), glycerol ($C_3H_8O_3$, Kishida Chemicals, 99.8 %), and distilled water were used as starting materials to synthesize nickel hydroxide-based monolithic gels. In addition, we used poly(acrylic acid) (PAA, Sigma-Aldrich, 35 wt% in $H_2O$, average molecular weight of 100,000) as a phase separation inducer as well as a network former, trimethylene oxide (TMO, Acros Organics, >97 %) or propylene oxide (PO, Sigma-Aldrich,

99 %) as a gelation initiator, 2-propanol (IPA, Kishida Chemicals, >99 %) as a washing solvent, respectively.

The sample ID is named as Ni-*w*-*x*-*y*-*z*, where *w*, *x*, *y*, and *z* indicate either T or P (gelation initiator added, TMO or PO), total volume of water (in mL), volume of glycerol (in mL), and weight of PAA (solution, in gram), respectively. In a typical sample (Ni-T-1.35-0.2-1.0), 0.535 g of $NiCl_2 \bullet 6H_2O$ and 1.0 g of PAA were dissolved in 0.7 mL of distilled water and 0.2 mL of glycerol under an ambient condition, and then 0.44 mL of TMO was added to the solution at 30 ºC. After stirring the solution for 1 min, the glass tube was degassed by ultrasonication for 10 s. Samples with varied amounts of water (*x*), glycerol (*y*), PAA (*z*), or the gelation initiator (T or P) were synthesized; since PAA is 35 wt% in water, total volume of water is arranged to the fixed amount at 1.35 mL when the weight of PAA is changed. The solutions thus prepared were kept in a sealed container at 60 ºC for gelation. The wet gels were aged at 60 ºC for 48 h, and immersed in IPA at 60 ºC for 24 h for two times, then dried by evaporation at 40 ºC. The dried samples were then heat-treated up to 1000 ºC for 4 h with a heating rate of 5 ºC $min^{-1}$ in air or Ar atmosphere with a flowing rate of 1 L $min^{-1}$.

## 2.2. Characterization

Microstructural morphology was observed by a scanning electron microscope (SEM) (JSM-6060, JEOL, Ltd., Japan, with Pt coating). Thermogravimetric-differential thermal analysis (TG-DTA)

(Thermo plus EVO TG 8120, Rigaku Corp., Japan) was performed at a heating rate of 5 ºC $min^{-1}$ supplying air or Argon at a rate of 100 mL $min^{-1}$ from room temperature to 1000 ºC on 1.0-1.5 mg of ground samples in both conditions. Chemical bonding information was obtained by Fourier transform infrared absorption (FT-IR) (IR Affinity-1, Shimadzu Corp., Japan) using the KBr method; each spectrum was collected after 100 scans for the wavenumber range 400-4,000 $cm^{-1}$ at a resolution of 2 $cm^{-1}$. Raman spectra were measured by a Raman microscope (XploRa, HORIBA, Ltd., Japan). Mercury porosimetry (Poremaster 60-GT, Quantachrome Instruments, USA) was used to characterize the macropores. Nanometer-ranged pore structure was analyzed from nitrogen adsorption-desorption isotherms (Belsorp mini II, Bel Japan Inc., Japan). The specific surface area was estimated by the Brunauer-Emmett-Teller (BET) method. X-ray diffraction (XRD) patterns with Cu K radiation ( = 0.154 nm) (RINT-Ultima III, Rigaku Corp., Japan) was carried out from 10º to 90º to identify the crystalline phase.

## 3. Results and Discussion

### 3.1. Xerogels: Effect of Starting Compositions on Morphologies

The relationship between starting composition and obtained materials' morphologies is summarized in Table 1. In a sol-gel synthesis to produce monolithic porous materials, the choice of solvent is an important issue. The appearance of typical dried sample and SEM images of samples prepared with

varied concentration of solvents are shown in Figure 1. With decrease the relative amount of water (*x*) compared to that of glycerol (*y*), morphology changed from particle aggregation (Ni-T-1.55-0.0-1.0, Figure 1b) through co-continuous network (Ni-T-1.35-0.2-1.0, Figure 1c) to fine porous structure (Ni-T-0.95-0.6-1.0, Figure 1d). As shown in Figure 1c, well-defined macropores (pore size about 0.70 m) were formed, whereas there were limited amount of nanometer-sized pores, implying xerogels thus obtained possess predominantly macropores (mercury porosimetry results shown in Figure S1). As evidenced in the previous reports [29,30], since the glycerol is partly distributed to the gel phase after phase separation, there could be a strong interaction based on hydrogen bonding between the hydroxyl groups of glycerol and nickel hydroxide-based condensate, which plays an important role in forming the gel network. While gels with macroporous morphologies shown in SEM images from Figure 1b to Figure 1c are obtained in the presence of glycerol, only deformable fragile gels were obtained instead of monolithic rigid ones in the absence of glycerol, as depicted in Table 1. This fact strongly suggests that glycerol acts as a network-forming constituent and mechanically strengthens the gel network containing nanocrystals of nickel hydroxide. On the other hand, the structural transition from Figure 1c to Figure 1d can be better explained by the suppressed coarsening process of phase-separating domains owing to the higher viscosity of the solvent mixture rich in glycerol. Since the kinetic factor influences the development of phase-separating domains, the difference in viscosity affected the coarsening of the phase-separating structure, resulting in the finer morphology with the solvent with higher viscosity [30].

Thus, the use of glycerol is a key factor here to form homogeneous gel network as well as monolithic rigid gels by simultaneously controlling the sol-gel reaction and phase separation.

The SEM images of samples prepared with varied amount of PAA (*z*) are shown in Figure 2. Gelation did not occur in the absence of PAA (Ni-P-1.35-0.2-0.0), whereas the addition of PAA produced monolithic rigid gels and gelation time (shown inset) increased with the amount of PAA. Macroporous morphologies changed from fragmented network composed of particles ($z < 1.0$, Figure 2a-d) through smooth co-continuous skeletons (Ni-T-1.35-0.2-1.0, Figure 2e) to non-porous matrix in the micrometer scale (Ni-T-1.35-0.2-1.2, Figure 2f). To our experience so far, additives containing a functional group such as carboxyl or amide group play important roles in precisely controlling macro- and micro-morphology via liquid-phase synthesis [27,29,34,35]. Analysis by FT-IR for the typical as-dried sample indicates that PAA is preferentially distributed to the gel phase, as represented in Figure S2 [36]. Poly(acrylic acid) also interacts with nickel hydroxide-based condensate through hydrogen bonding between carboxyl group and hydroxyl group. Thus, the obtained gel networks consist essentially of nickel hydroxide-based condensate, glycerol, and PAA. Since the addition of PAA induced gelation, PAA acts as a gelation agent, which also behaves as a network-forming constituent to organize co-continuous skeletons. The morphological change shown in Figure 2 is explained by the relative volume ratio of “network-forming constituents” to the solvent phase; as amount of PAA increases, the gel fraction becomes larger and results in the change from fragmented skeleton to

continuous one, as depicted in Table 1.

In a sol-gel method using a proton scavenger, the degree of pH increase is one of the important factors in synthesizing homogeneous gels with controlled structure. In particular, the difference in the reactivity of the proton scavenger used leads to the changes in morphology, porous properties, and crystallinity [37]. When we prepared a sample using the same amount of PO instead of TMO (Ni-P-1.35-0.2-1.0), monolithic gels were obtained in about 15 min, which is faster than the case using TMO (Ni-T-1.35-0.2-1.0, about 5 h), whereas porous structure of xerogels was inhomogeneous (shown in Figure S3). In general, it is known that metal cation ($M^{X+}$) acts as an acid to promote the hydrolysis and condensation, and the tendency to form homogeneous gels decreases in the order of $X = 4 > 3 > 2$ when a proton scavenger is used as a gelation initiator [25]. Since the valence of metal cation influences the gel formation kinetics, quick gelation observed in the sample using PO led to the formation of inhomogeneous structure due to its much higher reactivity and resultant higher supersaturation than the case of TMO [37]. In the present study, it is essential for preparing xerogels with homogeneous micrometer-ranged morphology to choose the appropriate proton scavenger, which promotes kinetically moderate gelation in parallel with phase separation.

### 3.2. Heat-Treatment under Air and Argon: Crystallization and Hierarchically Pores

All heat-treatment were carried out for the typical xerogel sample (Ni-T-1.35-0.2-1.0). Figure 3a

shows SEM images of samples after heating under air at 200 ºC and 300 ºC, and Figure 3b represents XRD patterns of them. While the continuous macroporous structures were retained even after the heat-treatment, the monoliths were cracked into small pieces. As shown in Figure 3b, there were no identifiable diffraction peaks below 200 ºC indicating an amorphous state, however, peaks ascribed to nickel oxide (NiO), which is the most stable oxide phase, appeared at 300 ºC. The TG-DTA curves obtained under air are shown in Figure S4 as solid lines, where weight loss and two exothermic peaks from 300 ºC to 400 ºC were observed. These peaks indicate that the pyrolysis of PAA within the skeleton and crystallization into nickel oxide occur in the temperature range, which agrees with the XRD results in Figure 3b. A heat treatment under air on as-dried xerogel samples composed of amorphous hydroxide-based condensate containing organic species induces the crystallization into stable oxide phase accompanied by the pyrolysis of organic species, which causes a considerable volume shrinkage resulting in the collapse of monolithic and co-continuous structures [29]. Since pyrolysis of organic species in xerogels led to the morphological changes, detailed information on the macropore structure could not be obtained.

On the other hand, heat-treatment under argon flow gave different features; Figure 4a shows SEM images of the samples heated under argon at 400 ºC and 1000 ºC, while Figure 4b represents mercury porosimetry results. It is found from Figure 4 that both co-continuous structures and monolithic forms were perfectly preserved with isotropic shrinkage, where macropore size of the samples decreased from

0.70 m for as-dried sample to ~0.43 m for heat-treated ones with increasing heating temperature, as shown in Figure 4b. Evolutions of XRD patterns of the samples heat-treated under argon are depicted in Figure 5a. The heat treatment above 300 ºC brought about strong peaks attributed to metallic nickel, and the crystallinity increased at higher temperatures. Their respective crystallite diameters estimated by the Scherrer's equation at 2 = 44.5º were: 5.8 nm at 300 ºC, 7.5 nm at 400 ºC, 13 nm at 600 ºC, 35 nm at 800 ºC, and 46.1 nm at 1000 ºC. Considering the above discussion that organic species cooperatively compose the gel network, the heat-treatment under an inert gas flow formed carbon derived from the organic species that are homogeneously distributed within the gel skeletons. The finely dispersed carbon thus formed is able to work as a reductant; "carbothermal reduction" takes place to form fully reduced crystalline phase, metallic nickel [38]. Since the carbon from organic species generates a strong reducing atmosphere [29,30,38], nickel hydroxide-based xerogel were reduced to the metal phase. The TG-DTA curves performed under an argon flow condition are represented in Figure S4 as dashed lines. Unlike that examined under air flow, two-step weight losses around 400 ºC and between 400 ºC and 1000 ºC were observed; the first originates from the crystallization into metallic Ni, and the second could be explained by the gradual pyrolysis of carbon. The presence of carbon in the network was confirmed by Raman spectra, as depicted in Figure 5b. Two distinct bands at ~1,350 $cm^{-1}$ and at ~1,600 $cm^{-1}$ were found that are ascribed to defected carbons (D band) and graphitic carbons (G band), respectively. Considering the formation of metallic nickel particles evidenced by XRD shown

in Figure 5a, it is concluded that obtained samples are nickel/carbon (Ni/C) "composites" instead of carbides. The carbon contents of the Ni/C composites were evaluated by TG curves for Ni/C samples under an air flow, as shown in Figure S5. The weight loss around 400 ºC-600 ºC is attributed to the pyrolysis of carbon. Taking the oxidation reaction from metallic nickel to nickel oxide (NiO) by the heat-treatment under air into account, the carbon contents of Ni/C samples can be estimated as summarized in Table S1. The Ni/C composites prepared here contain ~50 wt% carbon, and the contents slightly decrease with increasing heat-treatment temperature.

The nanometer-sized pore properties of Ni/C composites were investigated by nitrogen adsorption-desorption analysis in Figure 6. Nanometer-sized pores are formed as interstices between primary particles as well as the result of pyrolysis of carbon within the skeletons, which give high BET specific surface areas: 14 $m^2 g^{-1}$ at 300 ºC, 191 $m^2 g^{-1}$ at 400 ºC, 168 $m^2 g^{-1}$ at 600 ºC, 129 $m^2 g^{-1}$ at 800 ºC, and 63 $m^2 g^{-1}$ at 1000 ºC, respectively. Revealed from two-step decreases in TG curves under argon flow in Figure S4, a large amount of micropores derived from interstices were produced at the first weight loss due to the crystallization into metallic Ni from 300 ºC to 400 ºC, while the amount of pores decreased because heat-treatment enlarged crystallite size of metallic nickel to eliminate micropores shown in Figure 5a. Since the heat evolution led to further crystallization to change the size and amount of pores, different sized pores were formed through the heat-treatment (shown in Figure S6, the distribution of mesopores estimated by the Barrett-Joyner-Halenda method). Thus obtained

monolithic Ni/C possesses hierarchical pores; well-defined macropores and nanometer-sized pores to give high specific surface area.

## 4. Conclusions

Monolithic nickel hydroxide-based xerogels and nickel/carbon (Ni/C) composites with hierarchical pores have been successfully prepared by a facile sol-gel technique accompanied by phase separation. Nickel hydroxide-based xerogels that possess well-defined macropores about 0.70 m were characterized to be amorphous by XRD. Subsequent heat-treatment in air brought about the crystallization of NiO with collapse of monolithic form. On the other hand, heat-treatment under argon flow led to the formation of Ni/C composites with well-defined macropores and nanometer-sized pores to contribute high specific surface areas without spoiling the monolithic forms. The facile and versatile synthetic route has a potential to be extended to various monolithic inorganic materials, which include oxide, carbide, and nitride as well as metallic materials, with well-controlled pores based on divalent metal hydroxides.

**Supplementary Data Available**.

Mercury porosimetry, Nitrogen adsorption-desorption, FT-IR, SEM images, TG-DTA

**References**


[1] H. Sato, T. Minami, S. Takata, T. Yamada, Thin Solid Films (236) 1993, 27-31.

[2] J. A. Dirksen, K. Duval, T. A. Ring, Sens. Actuators, B (80) 2001, 106-115.

[3] D. J. Lensveld, J. G. Mesu, A. J. Dillen, K. P. de Jong, Microporous Mesoporous Mater. (44) 2001, 401-407.

[4] D. Das, M. Pal, E. D. Bartolomeo, E. Traversa, D. Chakravorty, J. Appl. Phys. (88) 2000, 6856-6860.

[5] J. Estellé, P. Salagre, Y. Cesteros, M. Serra, F. Medina, J. E. Sueiras, Solid State Ionics (156) 2003, 233-243.

[6] Y. Li, B. Zhang, X. Xie, J. Liu, Y. Xu, W. Shen, J. Catal. (238) 2006, 412-424.

[7] R. Ojani, J. B. Raoof, S. R. H. Zavvarmahalleh, Electrochim. Acta (53) 2008, 2402-2407.

[8] A. Sharma, H. Nakagawa, K. Miura, Fuel (85) 2006, 2396-2401.

[9] S. F. Wang, F. Xie, R. F. Hu, Sens. Actuators, B (123) 2007, 495-500.

[10] M. Zieliński, R. Wojcieszak, S. Monteverdi, M. Mercy, M. M. Bettahar, Int. J. Hydrogen Energy (32) 2007, 1024-1032.

[11] S. D. Tiwari, K. P. Rajeev, Thin Solid Films (505) 2006, 113-117.

[12] G. A. Niklasson, C. G. Granqvist, J. Mater. Chem. (17) 2007, 127-156.

[13] D. Wang, C. Song, Z. Hu, X. Fu, J. Phys. Chem. B (109) 2005, 1125-1129.

[14] K. C. Liu, M. A. Anderson, J. Electrochem. Soc. (143) 1996, 124-130.

[15] C. Yuan, X. Zhang, L. Su, B. Gao, L. Shen, J. Mater. Chem. (19) 2009, 5772-5777.

[16] D. H. Chen, S. H. Wu, Chem. Mater. (12) 2000, 1354-1360.

[17] S. H. Wu, D. H. Chen, J. Colloid Interface Sci. (259) 2003, 282-286.

[18] D. H. Chen, C. H. Hsieh, J. Mater. Chem. (12) 2002, 2412-2415.

[19] Y. Yang, S. Lim, G. Du, Y. Chen, D. Ciuparu, G. L. Haller. J. Phys. Chem. B (109) 2005, 13237-13246.

[20] M. S. Wu, Y. A. Huang, C. H. Yang, J. J. Jow, Int. J. Hydrogen Energy (32) 2007, 4153-4159

[21] K. Nakanishi, J. Porous Mater. (4) 1997, 67-112.

[22] H. Minakuchi, K. Nakanishi, N. Soga, N. Ishizuka, N. Tanaka, Anal. Chem. (68) 1996, 3498-3501.

[23] N. Nakamura, R. Takahashi, S. Sato, T. Sodesawa, S. Yoshida, Phys. Chem. Chem. Phys. (2) 2000, 4983-4990.

[24] A. E. Gash, T. M. Tillotson, J. H. Satcher Jr., J. F. Poco, L. W. Hrubesh, R. L. Simpson, Chem. Mater. (13) 2001, 999-1007.

[25] A. E. Gash, T. M. Tillotson, J. H. Satcher Jr., L. W. Hrubesh, R. L. Simpson, J. Non-Cryst. Solids (285) 2001, 22-28.

**Figure captions**

[27] Y. Tokudome, A. Miyasaka, K. Nakanishi, T. Hanada, J. Sol-Gel Sci. Technol. (57) 2011, 269-278.

[28] G. Hasegawa, Y. Ishihara, K. Kanamori, K. Miyazaki, Y. Yamada, K. Nakanishi, T. Abe, Chem. Mater. (23) 2011, 5208-5216.

[29] Y. Kido, K. Nakanishi, A. Miyasaka, K. Kanamori, Chem. Mater. (24) 2012, 2071-2077.

[30] Y. Kido, K. Nakanishi, K. Kanamori, RSC Adv. (published online, DOI: 10.1039/C3RA22481C)

[31] A. E. Gash, J. H. Satcher Jr., R. L. Simpson, J. Non-Cryst. Solids (350) 2004, 145-151.

[32] Y. P. Gao, C. N. Sick, L. J. Hope-Weeks, Chem. Mater. (19) 2007, 6007-6011.

[33] K. Nakanishi, N. Soga, J. Non-Cryst. Solids (139) 1992, 1-13.

[34] J. Rubio, E. Matijević, J. Colloid Interface Sci. (68) 1979, 408-421.

[35] J. Wen, V. J. Vasudevan, G. J. Wilkes, J. Sol-Gel Sci. Tecnol. (5) 1995, 115-126.

[36] R. M. Silverstein, F. X. Webster, D. J. Kiemle, Infrared Spectrometry: Spectrometric Identification of Organic Compounds, seventh ed., John Wiley & Sons, Inc., New York, 2005, pp. 99-101.

[37] A. E. Gash, J. H. Satcher Jr., R. L. Simpson, Chem. Mater. (15) 2003, 3268-3275.

[38] B. V. L'vov, Thermochim. Acta (360) 2000, 109-120.

**Figure captions**

Figure 1. (a) Appearance of typical xerogel sample, and SEM images of xerogel samples with varied amounts of solvent; (b) Ni-T-1.55-0.0-1.0, (c) Ni-T-1.35-0.2-1.0, and (d) Ni-T-0.95-0.6-1.0, respectively.

Figure 2. SEM images of xerogel samples with varied amount of PAA added; (a) Ni-T-1.35-0.2-0.2, (b) Ni-T-1.35-0.2-0.4, (c) Ni-T-1.35-0.2-0.6, (d) Ni-T-1.35-0.2-0.8, (e) Ni-T-1.35-0.2-1.0, and (f) Ni-T-1.35-0.2-1.2, respectively. Inset indicates gelation time.

Figure 3. (a) SEM images of samples heat-treated under air at (i) 200 ºC and (ii) 300 ºC. (b) XRD patterns of the samples at different temperatures. Open circles indicate nickel oxide (NiO).

Figure 4. (a) SEM images of the samples heat-treated under argon at (i) 400 ºC and (ii) 1000 ºC. Inset indicates appearance of the samples. (b) Mercury porosimetry results of the as-dried xerogel sample (open circle, solid line), the sample heat-treated under argon at 400 ºC (open triangle, dashed line), and at 1000 ºC (open square, dotted line), respectively.

Figure 5. (a) XRD patterns and (b) Raman spectra of the samples heat-treated under argon at different temperatures. Open squares in (a) indicate metallic nickel (Ni).

Figure 6. Nitrogen adsorption-desorption isotherms of the samples heat-treated under argon at different temperatures; open triangles: 300 ºC, open circles: 400 ºC, closed circles: 600 ºC, open squares: 800 ºC, and closed squares: 1000 ºC, respectively.

Figure1

Click here to download high resolution image

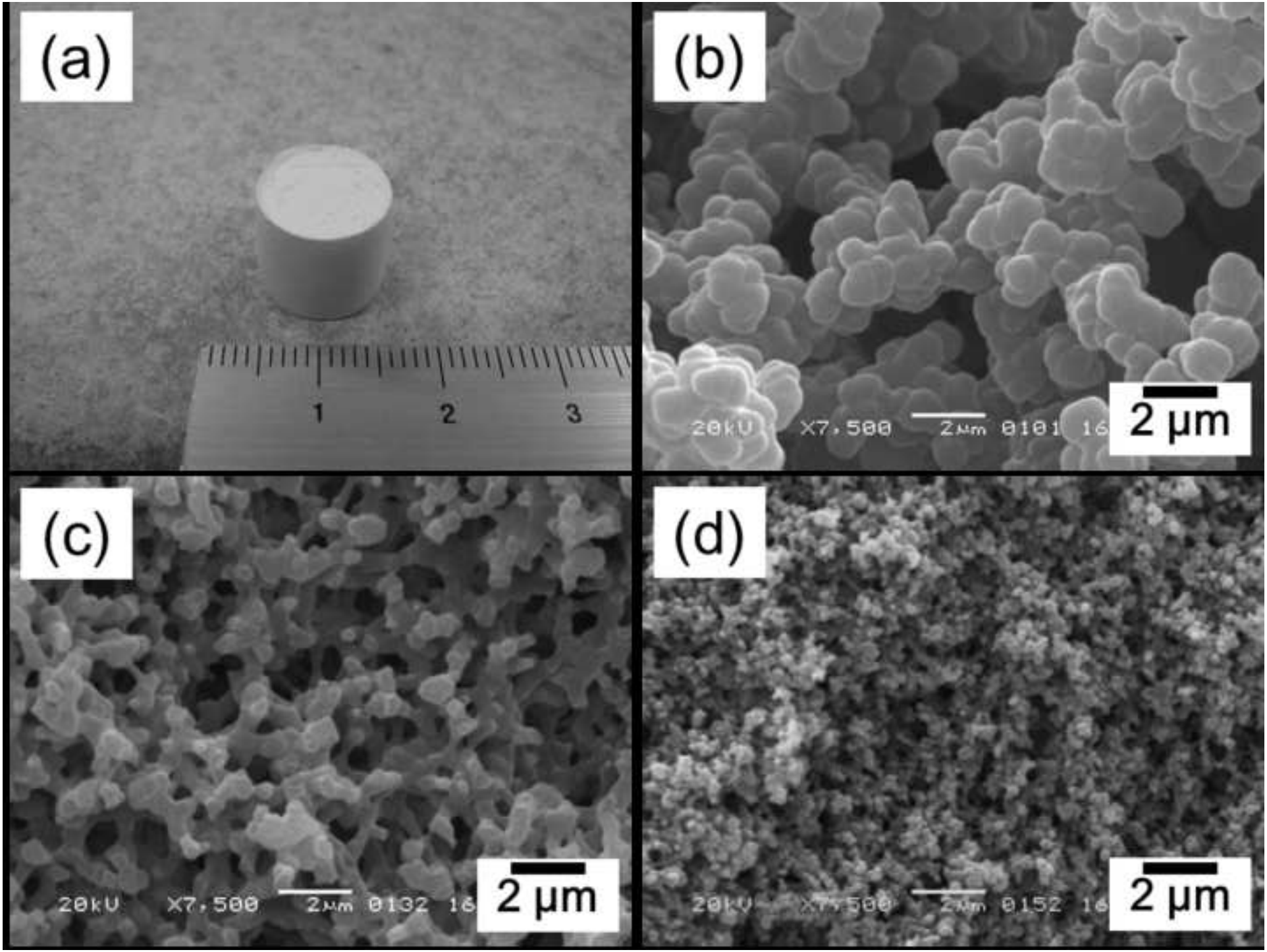

Figure2
Click here to download high resolution image

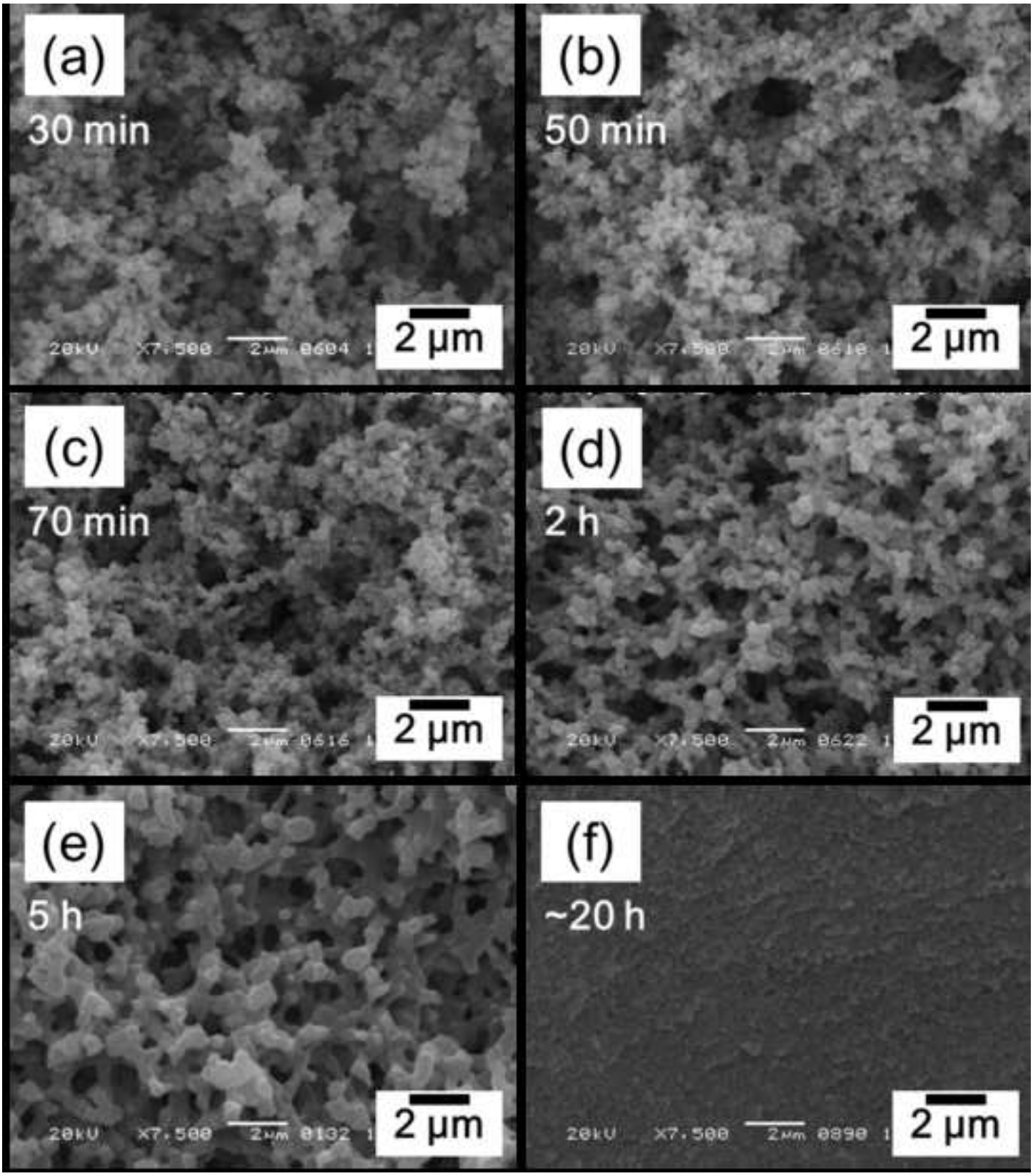

Figure3

Click here to download high resolution image

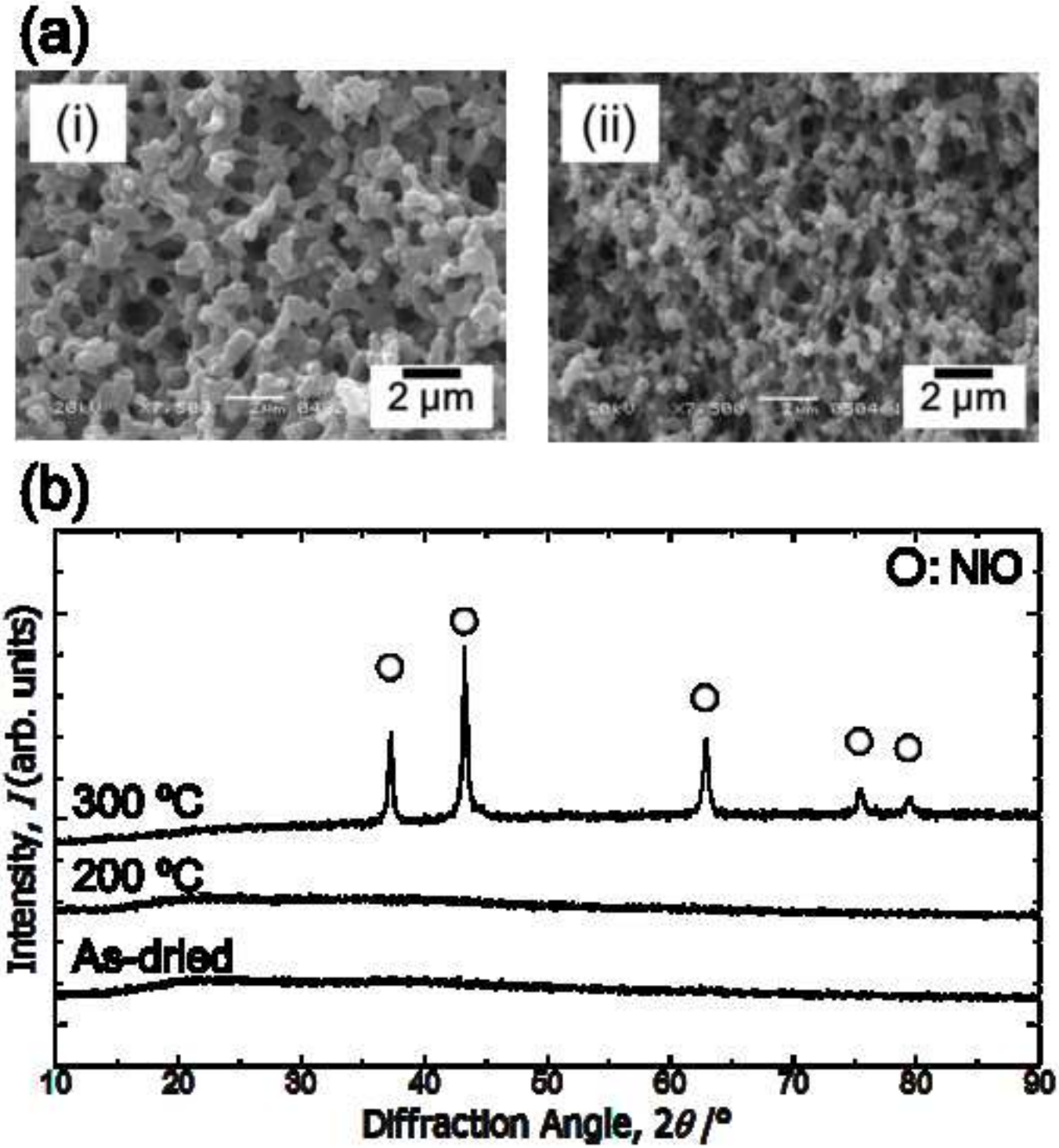

Figure4

Click here to download high resolution image

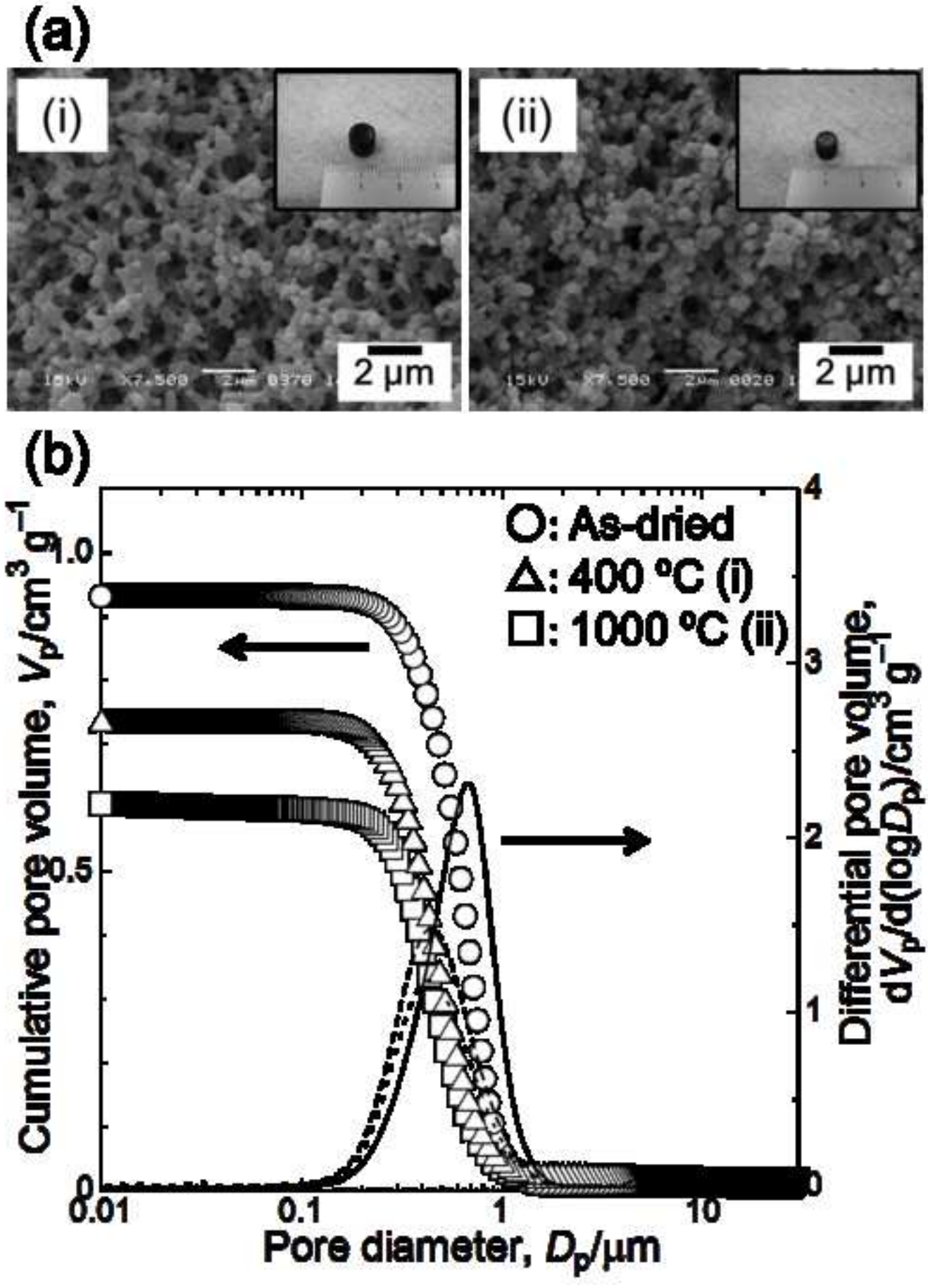

Figure5

Click here to download high resolution image

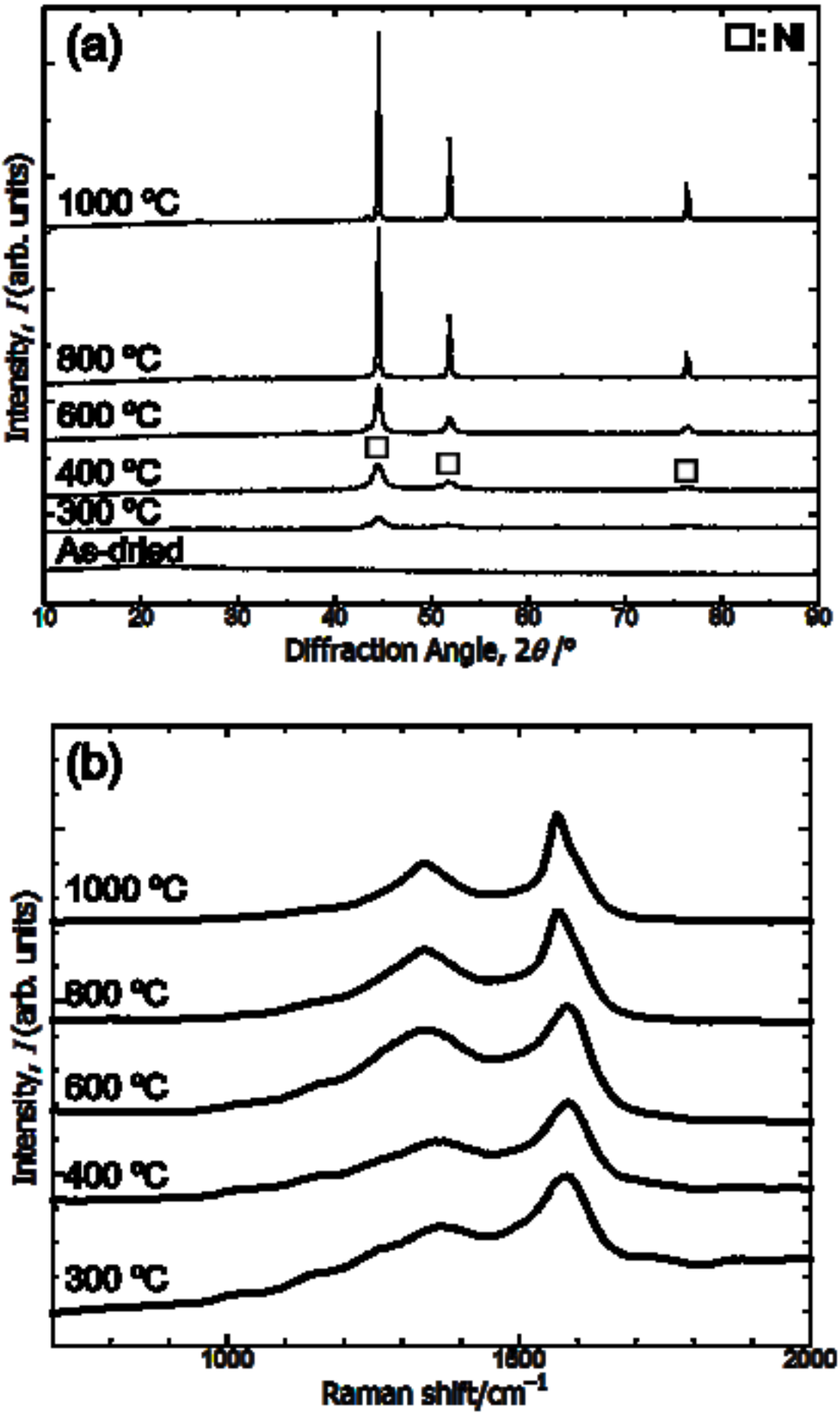

Figure6

Click here to download high resolution image

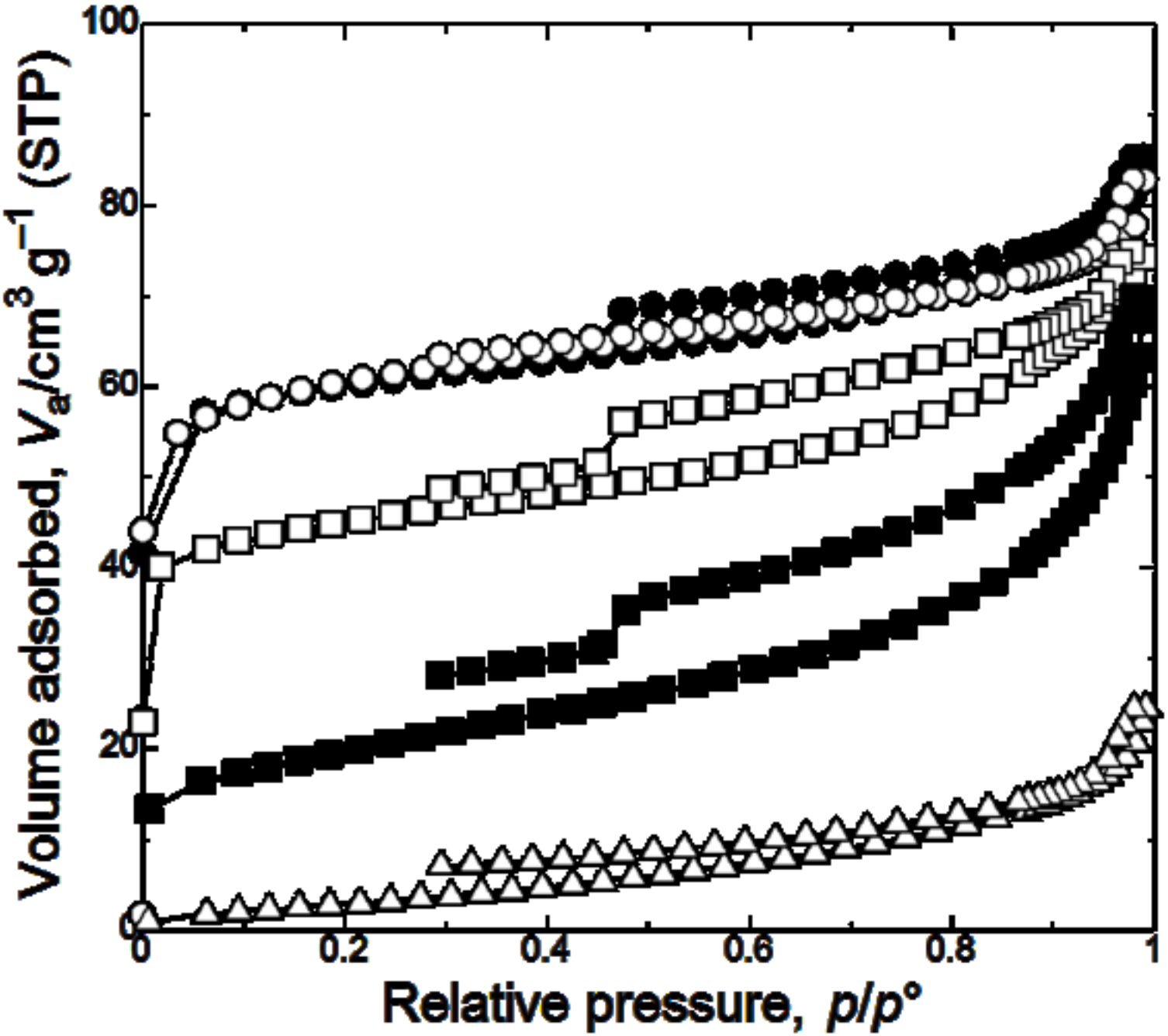

**Tables:**

**Table 1. Summary of microstructure and macroscopic appearance of the obtained samples**

| Sample ID | Microstructure | Monolithic Form (Y/N) |
|---|---|---|
| Ni-T-1.55-0.0-1.0 | Fragmented skeleton composed of large particle | N |
| Ni-T-1.35-0.2-1.0 | Co-continuous | Y |
| Ni-T-0.95-0.6-1.0 | Fine co-continuous | Y |
| Ni-T-1.35-0.2-0.0 | — | N (No gelation) |
| Ni-T-1.35-0.2-0.2 | Fragmented skeleton composed of fine particle | Y |
| Ni-T-1.35-0.2-0.4 | Fragmented skeleton composed of fine particle | Y |
| Ni-T-1.35-0.2-0.6 | Fragmented skeleton composed of fine particle | Y |
| Ni-T-1.35-0.2-0.8 | Fragmented skeleton ~ Co-continuous | Y |
| Ni-T-1.35-0.2-1.2 | Non-porous | Y |
| Ni-P-1.35-0.2-1.0 | Inhomogeneous co-continuous | Y |

Supplementary Data for

# Hierarchically Porous Nickel/Carbon Composite Monoliths Prepared by Sol-Gel Method from an Ionic Precursor

Yasuki KIDO, Kazuki NAKANISHI,* Nao OKUMURA and Kazuyoshi KANAMORI

Department of Chemistry, Graduate School of Science, Kyoto University,
Kitashirakawa, Sakyo-ku, Kyoto 606-8502, Japan.

E-mail: kazuki@kuchem.kyoto-u.ac.jp

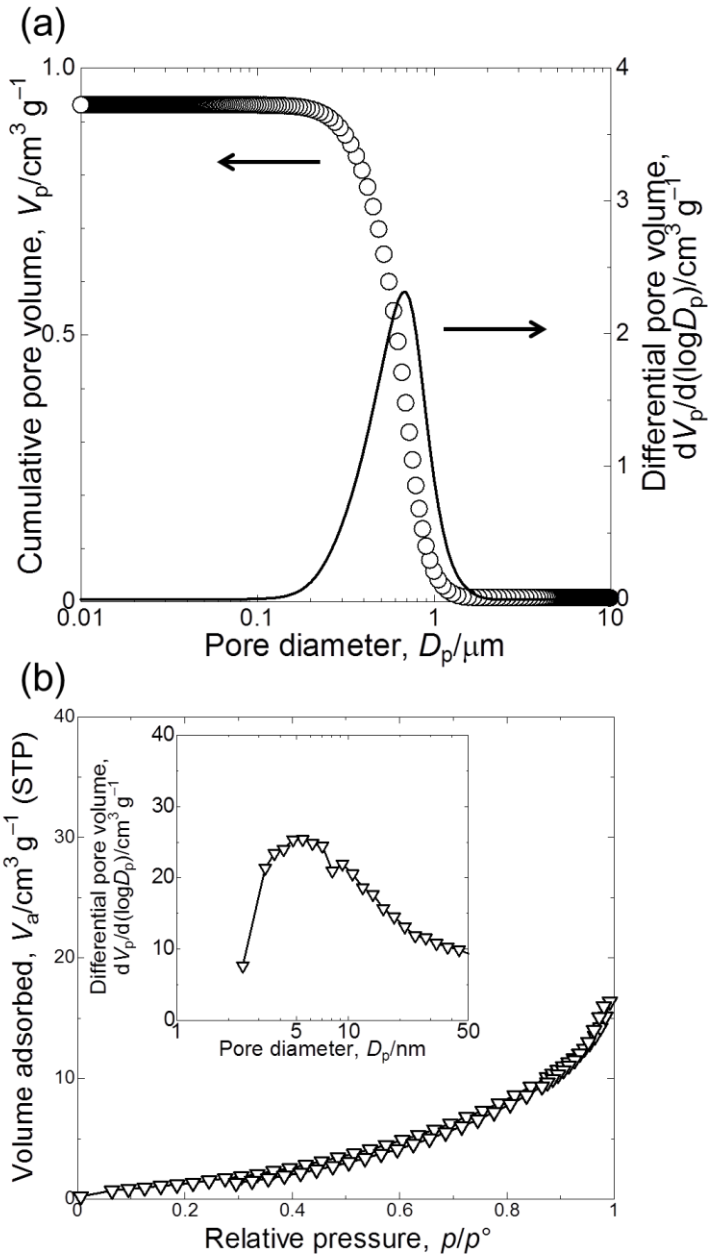


Figure S1. (a) The result of mercury porosimetry and (b) the nitrogen adsorption-desorption isotherm of a typical xerogel sample (Ni-T-1.35-0.2-1.0). Inset of (b) indicates pore size distribution estimated by the BJH method.

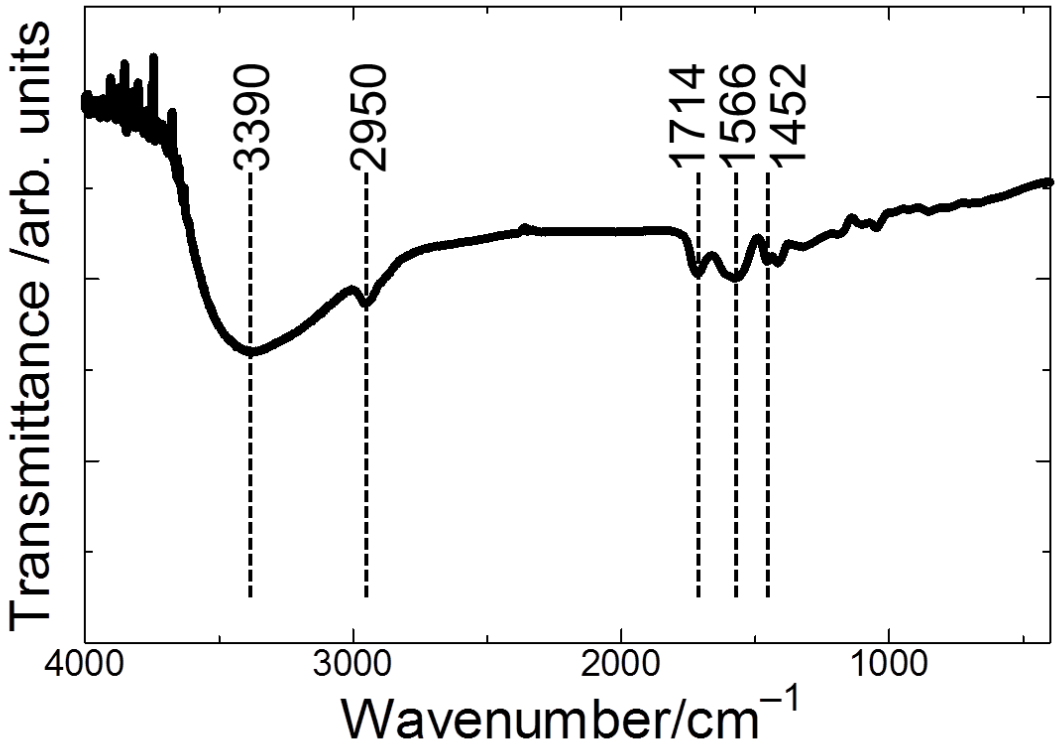


Figure S2. FT-IR spectrum of a typical xerogel sample (Ni-T-1.35-0.2-1.0). Dashed lines indicate absorptions by the following bonds; O-H for 3,390 $cm^{-1}$, C=O for 1,714 $cm^{-1}$, $COO^-$ for 1,566 $cm^{-1}$, and $CH_2$ for 2,950 $cm^{-1}$ and 1,452 $cm^{-1}$, respectively.

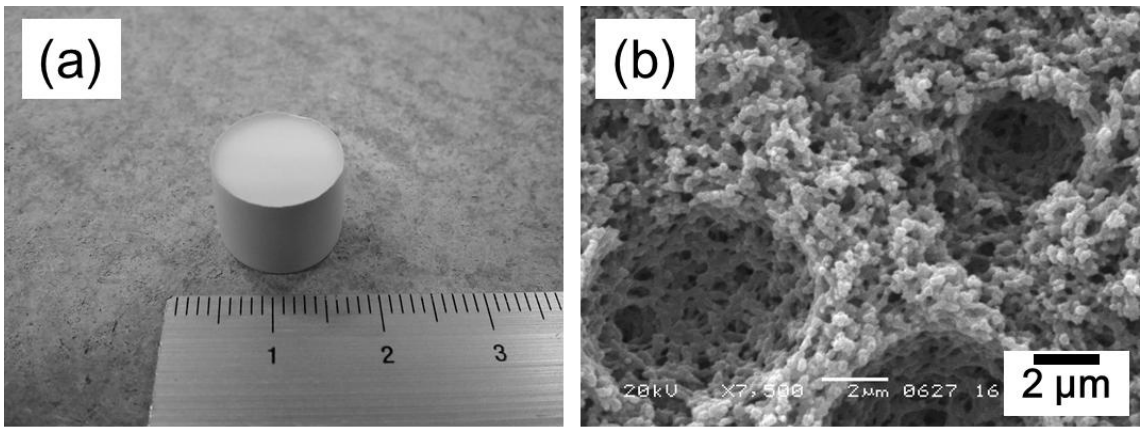


Figure S3. (a) Appearance and (b) an SEM image of a xerogel sample prepared with PO instead of TMO (Ni-P-1.35-0.2-1.0).

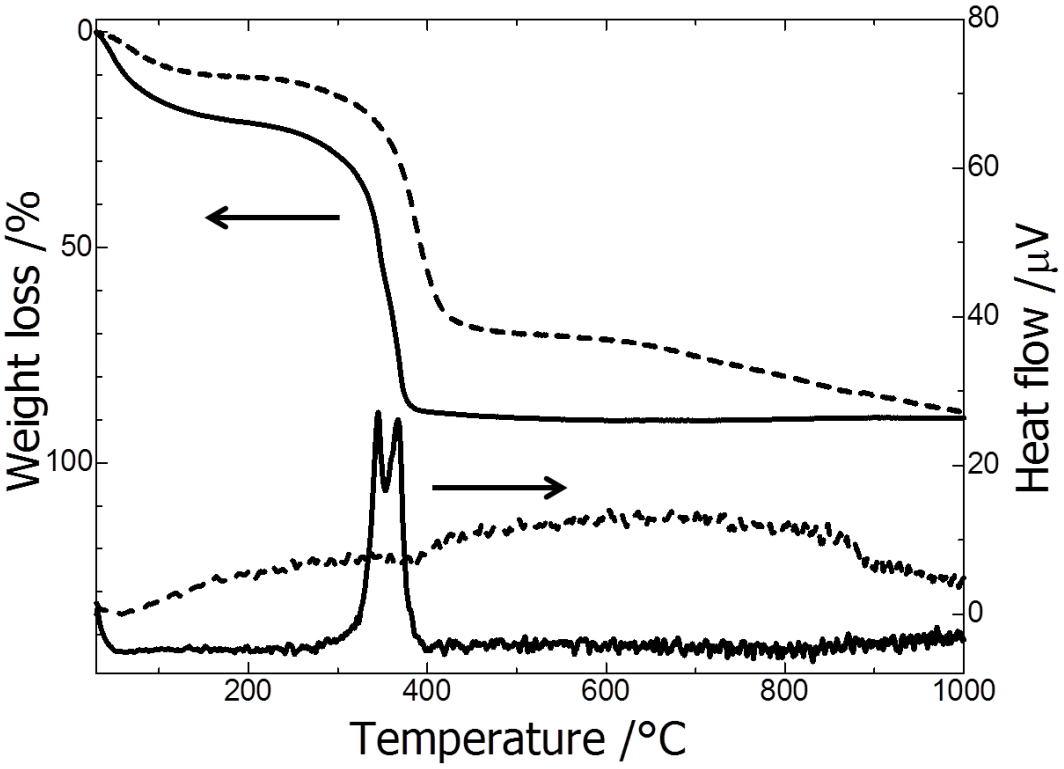


Figure S4. TG-DTA curves obtained under air flow (solid lines) and argon flow (dashed lines) for typical xerogel sample (Ni-T-1.35-0.2-1.0).

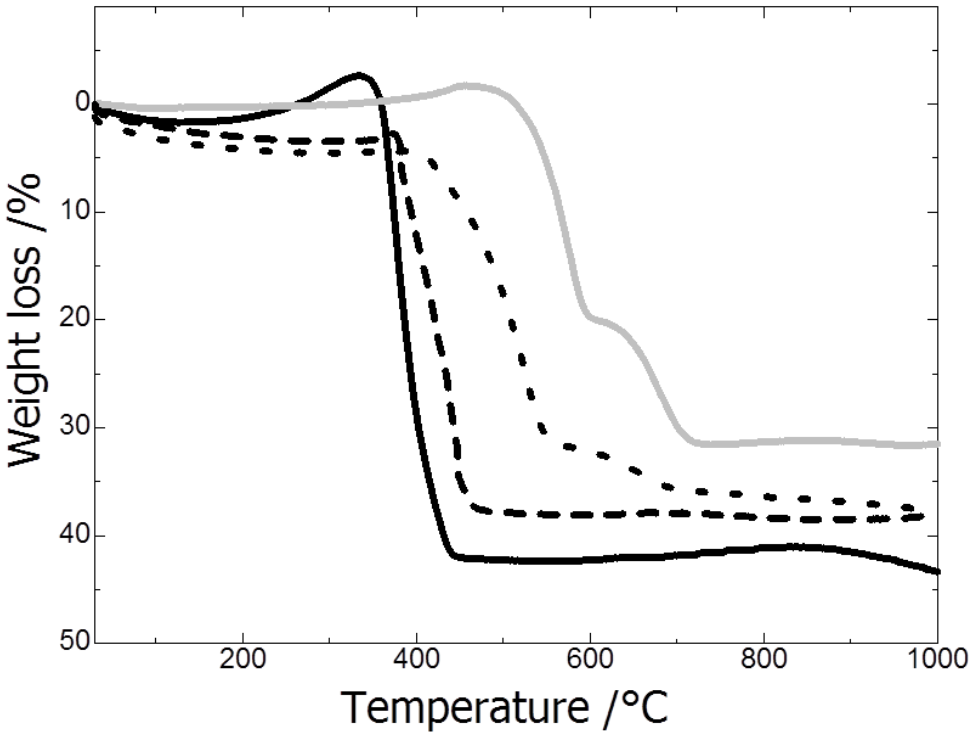


Figure S5. TG curves performed under air flow for the Ni/C composite samples obtained at different temperatures; solid line: 400 ºC, dashed line: 600 ºC, dotted line: 800 ºC, and gray line: 1000 ºC, respectively.

Table S1. Carbon contents of the Ni/C samples estimated from TG curves in Fig. S5.

| Heat-treatment temperature | carbon content / wt% |
|---|---|
| 400 ºC | 54 |
| 600 ºC | 51 |
| 800 ºC | 49 |
| 1000 ºC | 46 |

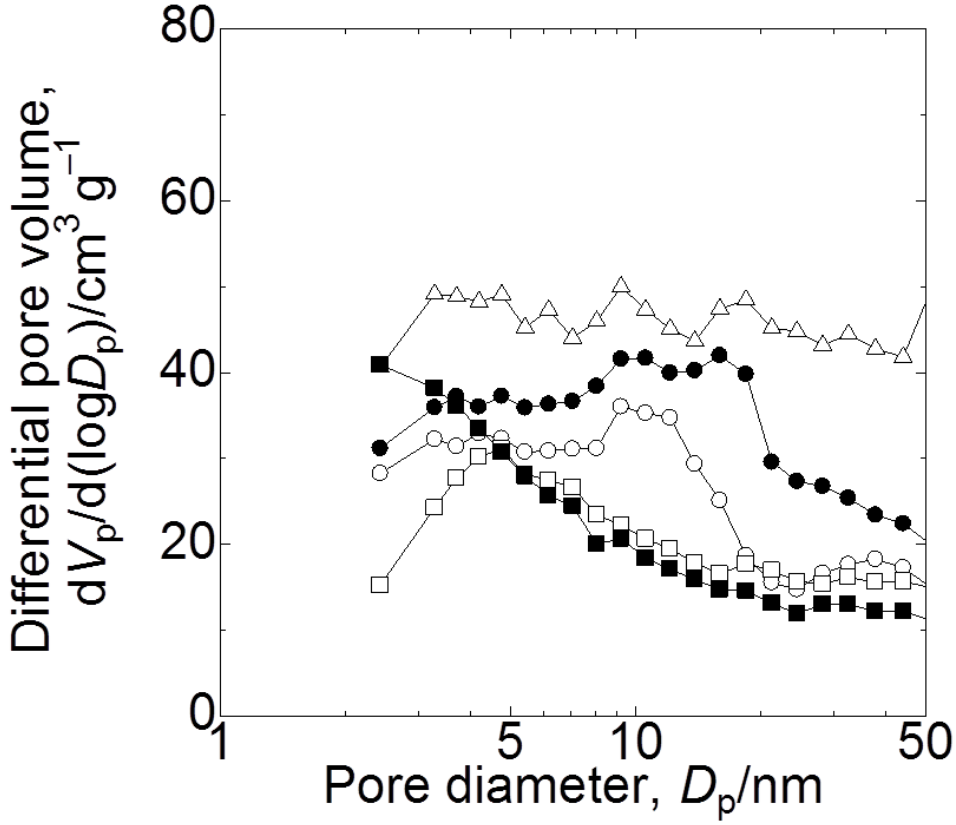


Figure S6. Pore size distribution estimated by the BJH method from nitrogen adsorption-desorption isotherms on the samples heat-treated under argon at different temperatures; open triangles: 300 ºC, open circles: 400 ºC, closed circles: 600 ºC, open squares: 800 ºC, and closed squares: 1000 ºC, respectively.